Antenna currents for optimal Q, superdirectivity, and radiation patterns using convex optimization

Gustafsson, Mats; Nordebo, Sven

2012

CODEN:LUTEDX/(TEAT-7216)/1-21/(2012)

Antenna currents for optimal Q, superdirectivity, and radiation patterns using convex optimization

Mats Gustafsson and Sven Nordebo

Electromagnetic Theory
Department of Electrical and Information Technology
Lund University
Sweden

Mats Gustafsson
mats.gustafsson@eit.lth.se

Department of Electrical and Information Technology
Electromagnetic Theory
Lund University
P.O. Box 118
SE-221 00 Lund
Sweden

Sven Nordebo
sven.nordebo@lnu.se

School of Computer Science, Physics and Mathematics
Linnaeus University
SE-351 95 Växjö
Sweden

Editor: Gerhard Kristensson

Abstract

The high Q-factor (low bandwidth) and low efficiency make the design of small antennas challenging. Here, convex optimization is used to determine current distributions that give upper bounds on the antenna performance. Optimization formulations for maximal gain Q-factor quotient, minimal Q-factor for superdirectivity, and minimum Q for given far-field are presented. The effects of antennas embedded in structures are also discussed. The results are illustrated for planar geometries.

1 Introduction

There are many advanced small antennas designs, such as folded helices, folded meander lines, and concepts based on metamaterials, fractals, and genetic algorithms. The high Q-factor (low bandwidth) and low efficiency make the design of small antennas challenging as the Q-factor, efficiency, and radiation resistance must be controlled simultaneously [7, 19]. It is well known that the antenna performance deteriorates with decreasing physical size (measured in wavelengths) of the antenna. The fundamental trade-off between performance and size is expressed by physical bounds. Physical bounds are useful because they provide bounds on the performance based solely on the shape and the size of the design volume.

Chu [8] used the stored and radiated energies outside a sphere that circumscribes the antenna to determine physical bounds on the Q-factor, Q, see also [28] for an overview. The stored energy in the interior of the sphere was added in [25]. Physical bound on the directivity Q-factor quotient D/Q were introduced for arbitrary sized and shaped antennas in [12, 13] under the assumption of $Q \gg 1$. Related bounds on the Q-factor are investigated for small antennas in [27, 29] and for finite sizes in [7]. The bounds in [12–14, 27, 29] are similar for the case of small dipole antennas composed of non-magnetic materials. In [14], optimal currents and physical bounds on D/Q are formulated as an optimization problem using the expressions for the stored energies presented by Vandenbosch [26], see also [9, 21]. The optimization problem in [14] is solved with a Lagrangian formulation.

Here, convex optimization [5, 15] is used to reformulate the optimization problem in [14]. This generalizes the optimization problem to include both the stored electric and magnetic energies. Moreover, it is shown that convex optimization offers many new possibilities to derive physical bounds on antennas. Here, we present results for minimum Q of superdirective antennas and minimum Q for antennas with a prescribed far field. We also illustrate how antennas embedded in metallic structures can be included in the bounds. The presented results are for arbitrary shaped structures but restricted to antennas composed of non-magnetic materials. The convex optimization problems are also only valid for functionals that are positive semidefinite. Here, we limit the size to approximately half a wavelength to obtain positive semidefinite energy expressions, see also [14]. It is also important to realize that the quality factor loses its practical meaning when Q is small. This restricts the interpretation of the presented results to $Q \gg 1$ that coincides with the size

restriction on the antennas considered in this paper.

Convex optimization is used in many areas [5] and it has been used extensively to determine array patterns [6]. The formulation as a convex optimization problem is advantageous as: it has a well-developed theory [5], there are efficient solvers [10], and the solution gives error estimates. Moreover, a local minimum is also the global minimum, so there is no risk of getting trapped in local minima. This is very different from general global optimization problems and one can often state that a problem is solved if it is formulated as a convex optimization problem [5].

This paper is organized as follows. The considered antenna parameters are introduced in Sec. 2. The used method of moments formulation is presented in Sec. 3. Sec. 4 contains the main results of the paper. It is divided into five subsections containing various convex optimization formulations giving antenna bounds. The results are also illustrated with bounds for planar rectangular geometries. The paper is concluded in Sec. 5.

2 Antenna parameters

We consider antennas in a volume V composed of non-magnetic materials with free space in the region exterior to V, see Fig. 1. The radiated field and stored energies are expressed in the antenna current $\boldsymbol{J}$ in V. The radiation intensity in the $\hat{\boldsymbol{k}}$-direction is $P(\hat{\boldsymbol{k}}) = \frac{\eta_0 k^2}{32\pi^2}|\boldsymbol{F}(\hat{\boldsymbol{k}})|^2$, where $\boldsymbol{F}$ is the tangential components of the radiation vector [22]

$$\boldsymbol{F}(\hat{\boldsymbol{k}}) = -\hat{\boldsymbol{k}} \times \int_V \hat{\boldsymbol{k}} \times \boldsymbol{J}(\boldsymbol{r}) \mathrm{e}^{\mathrm{j}k\hat{\boldsymbol{k}}\cdot\boldsymbol{r}} \,\mathrm{dV}, \tag{2.1}$$

η_0 denotes the free space impedance, $k = \omega/\mathrm{c}_0$ the wavenumber, c_0 the speed of light in free space, $\mathrm{j}^2 = -1$, and the time convention $\mathrm{e}^{\mathrm{j}\omega t}$ is used. The corresponding electric field is $\boldsymbol{E}(\boldsymbol{r}) = -\mathrm{j}k\eta_0 \frac{\mathrm{e}^{-\mathrm{j}kr}}{4\pi r}\boldsymbol{F}(\hat{\boldsymbol{r}})$, where $\boldsymbol{r}$ denotes the position vector, $\hat{\boldsymbol{r}} = \boldsymbol{r}/r$, and $r = |\boldsymbol{r}|$.

We also use the unit vector $\hat{\boldsymbol{e}}$, with $\hat{\boldsymbol{k}} \cdot \hat{\boldsymbol{e}} = 0$, to evaluate the partial radiation intensity for the polarization $\hat{\boldsymbol{e}}$. The field is linearly polarized for $|\hat{\boldsymbol{e}} \times \hat{\boldsymbol{e}}^*| = 0$ and circularly polarized for $|\hat{\boldsymbol{e}} \times \hat{\boldsymbol{e}}^*| = 1$, where the superscript, $*$, denotes the complex conjugate. This gives the partial radiation intensity $P(\hat{\boldsymbol{k}}, \hat{\boldsymbol{e}}) = \frac{\eta_0 k^2}{32\pi^2}|\hat{\boldsymbol{e}}^* \cdot \boldsymbol{F}(\hat{\boldsymbol{k}})|^2$, where

$$\hat{\boldsymbol{e}}^* \cdot \boldsymbol{F}(\hat{\boldsymbol{k}}) = \int_V \hat{\boldsymbol{e}}^* \cdot \boldsymbol{J}(\boldsymbol{r}) \mathrm{e}^{\mathrm{j}k\hat{\boldsymbol{k}}\cdot\boldsymbol{r}} \,\mathrm{dV}. \tag{2.2}$$

The partial directivity, $D(\hat{\boldsymbol{k}}, \hat{\boldsymbol{e}})$, is defined as [1]

$$D(\hat{\boldsymbol{k}}, \hat{\boldsymbol{e}}) = 4\pi \frac{P(\hat{\boldsymbol{k}}, \hat{\boldsymbol{e}})}{P_{\mathrm{rad}}}, \tag{2.3}$$

where P_{rad} is the total radiated power. The corresponding partial gain, $G(\hat{\boldsymbol{k}}, \hat{\boldsymbol{e}})$, is

$$G(\hat{\boldsymbol{k}}, \hat{\boldsymbol{e}}) = 4\pi \frac{P(\hat{\boldsymbol{k}}, \hat{\boldsymbol{e}})}{P_{\mathrm{rad}} + P_{\mathrm{loss}}}, \tag{2.4}$$

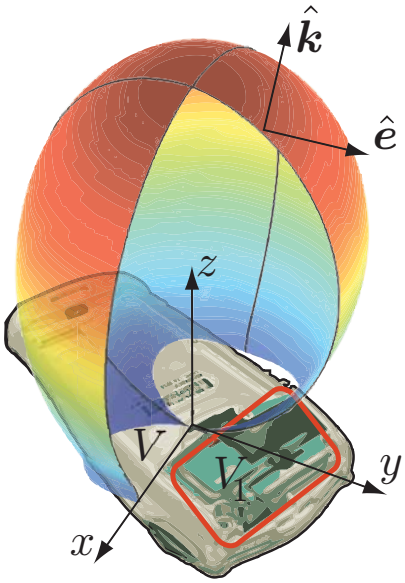

Figure 1: Structure in a region V with the antenna confined to $V_1 \subset V$. The antenna current $\boldsymbol{J}_1(\boldsymbol{r})$ for $\boldsymbol{r} \in V_1$ induces the current density $\boldsymbol{J}(\boldsymbol{r})$ for $\boldsymbol{r} \in V$ with a radiation pattern in the direction $\hat{\boldsymbol{k}}$ and polarization $\hat{\boldsymbol{e}}$.

where P_{loss} is the dissipated power in the antenna structure. The quality factor (or antenna Q), Q, is

$$Q = \frac{2\mathrm{c}_0 k \max\{W_{\text{e}}, W_{\text{m}}\}}{P_{\text{rad}} + P_{\text{loss}}}, \tag{2.5}$$

where W_{e} and W_{m} denote the stored electric and magnetic energies, respectively.

Follow the approach in [14] and use the results by Vandenbosch [26], to express the stored electric energy as $W_{\text{e}} = \widetilde{W}^{(\text{e})}_{\text{vac}} = \frac{\mu_0}{16\pi k^2} w^{(\text{e})}$, where

$$\begin{aligned} w^{(\text{e})}(\boldsymbol{J}) = &\int_V \int_V \nabla_1 \cdot \boldsymbol{J}(\boldsymbol{r}_1) \nabla_2 \cdot \boldsymbol{J}^*(\boldsymbol{r}_2) \frac{\cos(k|\boldsymbol{r}_1 - \boldsymbol{r}_2|)}{|\boldsymbol{r}_1 - \boldsymbol{r}_2|} \\ &- \frac{k}{2}\big(k^2 \boldsymbol{J}(\boldsymbol{r}_1) \cdot \boldsymbol{J}^*(\boldsymbol{r}_2) - \nabla_1 \cdot \boldsymbol{J}(\boldsymbol{r}_1) \nabla_2 \cdot \boldsymbol{J}^*(\boldsymbol{r}_2)\big) \sin(k|\boldsymbol{r}_1 - \boldsymbol{r}_2|)\, \mathrm{dV}_1\, \mathrm{dV}_2, \end{aligned} \tag{2.6}$$

and μ_0 is the permeability of free space. The stored magnetic energy is $W_{\text{m}} = \widetilde{W}^{(\text{m})}_{\text{vac}} = \frac{\mu_0}{16\pi k^2} w^{(\text{m})}$, where

$$\begin{aligned} w^{(\text{m})}(\boldsymbol{J}) = &\int_V \int_V k^2 \boldsymbol{J}(\boldsymbol{r}_1) \cdot \boldsymbol{J}^*(\boldsymbol{r}_2) \frac{\cos(k|\boldsymbol{r}_1 - \boldsymbol{r}_2|)}{|\boldsymbol{r}_1 - \boldsymbol{r}_2|} \\ &- \frac{k}{2}\big(k^2 \boldsymbol{J}(\boldsymbol{r}_1) \cdot \boldsymbol{J}^*(\boldsymbol{r}_2) - \nabla_1 \cdot \boldsymbol{J}(\boldsymbol{r}_1) \nabla_2 \cdot \boldsymbol{J}^*(\boldsymbol{r}_2)\big) \sin(k|\boldsymbol{r}_1 - \boldsymbol{r}_2|)\, \mathrm{dV}_1\, \mathrm{dV}_2. \end{aligned} \tag{2.7}$$

The corresponding expression for the total radiated power is $P_{\rm rad} = \frac{\eta_0}{8\pi k} p_{\rm rad}$ with

$$p_{\rm rad} = \int_V \int_V \big(k^2 \boldsymbol{J}(\boldsymbol{r}_1) \cdot \boldsymbol{J}^*(\boldsymbol{r}_2) - \nabla_1 \cdot \boldsymbol{J}(\boldsymbol{r}_1) \nabla_2 \cdot \boldsymbol{J}^*(\boldsymbol{r}_2)\big) \frac{\sin(k|\boldsymbol{r}_1 - \boldsymbol{r}_2|)}{|\boldsymbol{r}_1 - \boldsymbol{r}_2|} \,\mathrm{dV}_1 \,\mathrm{dV}_2. \quad (2.8)$$

The normalized quantities, $w^{(\mathrm{e})}, w^{(\mathrm{m})}$, in (2.7) and $p_{\rm rad}$ in (2.8) are introduced to simplify the optimization approach used in this paper. They have dimensions given by volume, m^3, times the dimension of $|\boldsymbol{J}|^2$, *i.e.*, $\mathrm{A}^2\mathrm{m}^{-4}$. The corresponding dimension of the radiation vector (2.1) is volume times the dimension of $|\boldsymbol{J}|$.

3 MoM formulation

We use local basis functions analogous with ordinary Method of Moments (MoM) solutions of the electric and magnetic integral equations [23] to approximate the radiation vector (2.1), stored energies (2.6), (2.7), and radiated power (2.8). Expand the current density in local basis functions

$$\boldsymbol{J}(\boldsymbol{r}) \approx \sum_{n=1}^{N} J_n \boldsymbol{\psi}_n(\boldsymbol{r}) \quad (3.1)$$

and introduce the $N \times 1$ matrix $\mathbf{J}$ with elements J_n to simplify the notation. The basis functions are assumed to be divergence conforming and having vanishing normal components at the boundary [23]. In this paper, we use piecewise linear basis functions on quadrilateral elements. The discretization is non-equidistant to capture edge singularities of the charge density.

The radiation vector projected on $\hat{\boldsymbol{e}}$, *cf.*, (2.2), defines the $N \times 1$ matrix $\mathbf{F}$ from

$$\hat{\boldsymbol{e}}^* \cdot \boldsymbol{F}(\hat{\boldsymbol{k}}) \approx \mathbf{F}^{\mathrm{H}} \mathbf{J} = \sum_{n=1}^{N} J_n \int_V \hat{\boldsymbol{e}}^* \cdot \boldsymbol{\psi}_n(\boldsymbol{r}) \mathrm{e}^{\mathrm{j}k\hat{\boldsymbol{k}}\cdot\boldsymbol{r}} \,\mathrm{dV}, \quad (3.2)$$

where the superscript, H, denotes the Hermitian transpose and the dependence of matrix $\mathbf{F}$ on $\hat{\boldsymbol{k}}$ and $\hat{\boldsymbol{e}}$ is suppressed. The normalized stored electric energy is approximated as

$$w^{(\mathrm{e})}(\boldsymbol{J}) \approx \sum_{m=1}^{N} \sum_{n=1}^{N} J_m^* w_{mn}^{(\mathrm{e})} J_n = \mathbf{J}^{\mathrm{H}} \mathbf{W}_{\mathrm{e}} \mathbf{J}, \quad (3.3)$$

where the $N \times N$ matrix $\mathbf{W}_{\mathrm{e}}$ has the elements

$$w_{mn}^{(\mathrm{e})} = \int_V \int_V \nabla_1 \cdot \boldsymbol{\psi}_m(\boldsymbol{r}_1) \nabla_2 \cdot \boldsymbol{\psi}_n(\boldsymbol{r}_2) \frac{\cos(k|\boldsymbol{r}_1 - \boldsymbol{r}_2|)}{|\boldsymbol{r}_1 - \boldsymbol{r}_2|} - \frac{k}{2} \big(k^2 \boldsymbol{\psi}_m(\boldsymbol{r}_1) \cdot \boldsymbol{\psi}_n(\boldsymbol{r}_2) - \nabla_1 \cdot \boldsymbol{\psi}_m(\boldsymbol{r}_1) \nabla_2 \cdot \boldsymbol{\psi}_n(\boldsymbol{r}_2)\big) \sin(k|\boldsymbol{r}_1 - \boldsymbol{r}_2|) \,\mathrm{dV}_1 \,\mathrm{dV}_2. \quad (3.4)$$

The normalized stored magnetic energy, $w^{(\mathrm{m})}(\boldsymbol{J}) \approx \mathbf{J}^{\mathrm{H}}\mathbf{W}_{\mathrm{m}}\mathbf{J}$, and the normalized radiated power, $p_{\mathrm{rad}}(\boldsymbol{J}) \approx \mathbf{J}^{\mathrm{H}}\mathbf{P}\mathbf{J}$ are defined analogously. The matrices $\mathbf{W}_{\mathrm{e}}$, $\mathbf{W}_{\mathrm{m}}$, and $\mathbf{P}$ are real-valued and symmetric. It is observed that $\mathbf{W}_{\mathrm{e}}$ can be indefinite for electrically large structures [14]. In the numerical examples in this paper, we restrict the electrical size to be approximately less than half a wavelength. The eigenvalues are also computed to verify that $\mathbf{W}_{\mathrm{e}}$ and $\mathbf{W}_{\mathrm{m}}$ are positive semidefinite. Here, it is observed that there can be a few negative eigenvalues. These negative eigenvalues are however due to the used finite numerical precision and their relative amplitude is 10^{-14} compared to the positive eigenvalues. We transform the matrices to become positive semidefinite by setting these eigenvalues to zero.

4 Convex optimization

We use convex optimization [5] to determine fundamental bounds on the antenna performance and their corresponding optimal current densities. We assume that $\mathbf{W}_{\mathrm{e}}$, $\mathbf{W}_{\mathrm{m}}$, and $\mathbf{P}$ are positive semidefinite for the electrical sizes considered in this paper. First, bounds on G/Q for small antennas as $ka \to 0$ are analyzed. It is followed by bounds on G/Q, Q for superdirective antennas, Q for antennas with prescribed far field, and G/Q for embedded antennas.

4.1 Bounds on G/Q for small antennas

Explicit bounds on the directivity Q-factor quotient, D/Q, (and equivalently G/Q) are presented for small antennas in [14]. The low-frequency expansion of the current density is $\boldsymbol{J} = \boldsymbol{J}^{(0)} + k\boldsymbol{J}^{(1)} + o(k)$ as $k \to 0$, where $\nabla \cdot \boldsymbol{J}^{(0)} = 0$ and $\nabla \cdot \boldsymbol{J}^{(1)} = -\mathrm{j}\rho$. The expansion simplifies the energy expressions (2.6) and (2.7) for small antennas [9, 14, 27]. The G/Q bound separates into electric dipoles, magnetic dipoles, and mixed modes antennas [14]. In [14], it is also shown that it is sufficient to consider surface currents for small antennas. The gain Q-factor quotient for small electric dipole antennas is bounded as [14]

$$\frac{G_{\mathrm{e}}}{Q_{\mathrm{e}}} \leq k^3 \max_{\rho} \frac{\left|\int_{\partial V} \hat{\boldsymbol{e}}^* \cdot \boldsymbol{r}\rho(\boldsymbol{r}) \,\mathrm{dS}\right|^2}{\int_{\partial V}\int_{\partial V} \frac{\rho^*(\boldsymbol{r}_1)\rho(\boldsymbol{r}_2)}{|\boldsymbol{r}_1-\boldsymbol{r}_2|} \,\mathrm{dS}_1 \,\mathrm{dS}_2} \tag{4.1}$$

subject to the constraint of zero total charge $\int_{\partial V} \rho(\boldsymbol{r}) \,\mathrm{dS} = 0$. Use that the quotient is invariant for scalings $\rho \to \alpha\rho$ to rewrite the bound (4.1) as the optimization problem

$$\begin{aligned} \text{minimize} \quad & \int_{\partial V}\int_{\partial V} \frac{\rho^*(\boldsymbol{r}_1)\rho(\boldsymbol{r}_2)}{4\pi|\boldsymbol{r}_1-\boldsymbol{r}_2|} \,\mathrm{dS}_1 \,\mathrm{dS}_2 \\ \text{subject to} \quad & \int_{\partial V} \hat{\boldsymbol{e}}^* \cdot \boldsymbol{r}\rho(\boldsymbol{r}) \,\mathrm{dS} = -1 \\ & \int_{\partial V} \rho(\boldsymbol{r}) \,\mathrm{dS} = 0, \end{aligned} \tag{4.2}$$

where 4π is included for convenience. Use basis functions similar to (3.1) to approximate the charge density as $\sum_{n=1}^{N} \rho_n \psi_n(\boldsymbol{r})$, let $\boldsymbol{\rho}$ denote the $N \times 1$ matrix with

elements ρ_n, and $\mathbf{W}_{\mathrm{e}}^{(0)}$, $\mathbf{f}$, $\mathbf{n}$ the corresponding matrix representations for the integral operators in (4.2), see also App. A. This gives the convex optimization problem

$$\begin{aligned} &\text{minimize} && \boldsymbol{\rho}^{\mathrm{H}}\mathbf{W}_{\mathrm{e}}^{(0)}\boldsymbol{\rho} \\ &\text{subject to} && \mathbf{f}_{\mathrm{e}}^{\mathrm{H}}\boldsymbol{\rho} = -1 \\ & && \mathbf{n}^{\mathrm{H}}\boldsymbol{\rho} = 0. \end{aligned} \tag{4.3}$$

This is a convex optimization problem in the form of a linearly constrained quadratic program [5] that *e.g.*, can be solved using `CVX` [10]. It is illustrative to use Lagrange multipliers [5, 24] to rewrite (4.3) as the linear system

$$\begin{pmatrix} \mathbf{W}_{\mathrm{e}}^{(0)} & \mathbf{f}_{\mathrm{e}} & \mathbf{n} \\ \mathbf{f}_{\mathrm{e}}^{\mathrm{H}} & 0 & 0 \\ \mathbf{n}^{\mathrm{H}} & 0 & 0 \end{pmatrix} \begin{pmatrix} \boldsymbol{\rho} \\ \gamma^{-1} \\ -C \end{pmatrix} = \begin{pmatrix} \mathbf{0} \\ -1 \\ 0 \end{pmatrix}, \tag{4.4}$$

where γ^{-1} and $-C$ are the Lagrange multipliers. The linear system (4.4) is identical with the MoM solution for the polarizability, $\gamma = \hat{\boldsymbol{e}} \cdot \boldsymbol{\gamma}_{\mathrm{e}} \cdot \hat{\boldsymbol{e}}$ using Galerkin's method, see App. A. This illustrates that the convex optimization can be numerically identical to the solution of the integral equation in [14].

The G/Q bound for the magnetic dipole case is reduced to an integral equation involving an arbitrary function in [14]. Here, we use a convex optimization problem to derive a simple linear system for the G/Q bound. The gain Q-factor quotient for a magnetic dipole antenna is bounded by

$$\frac{G_{\mathrm{m}}}{Q_{\mathrm{m}}} \leq \frac{k^3}{4\pi} \max_{\boldsymbol{J}} \frac{\left| \int_{\partial V} \frac{1}{2}((\hat{\boldsymbol{k}} \times \hat{\boldsymbol{e}}^*) \times \boldsymbol{r}) \cdot \boldsymbol{J}(\boldsymbol{r}) \, \mathrm{dS} \right|^2}{\int_{\partial V} \int_{\partial V} \frac{\boldsymbol{J}(\boldsymbol{r}_1) \cdot \boldsymbol{J}^*(\boldsymbol{r}_2)}{4\pi |\boldsymbol{r}_1 - \boldsymbol{r}_2|} \, \mathrm{dS}_1 \, \mathrm{dS}_2}, \tag{4.5}$$

where $\nabla \cdot \boldsymbol{J} = 0$. We scale $\boldsymbol{J}$ to reformulate (4.5) as the optimization problem

$$\begin{aligned} &\text{minimize} && \int_{\partial V} \int_{\partial V} \frac{\boldsymbol{J}^*(\boldsymbol{r}_1) \cdot \boldsymbol{J}(\boldsymbol{r}_2)}{4\pi |\boldsymbol{r}_1 - \boldsymbol{r}_2|} \, \mathrm{dS}_1 \, \mathrm{dS}_2 \\ &\text{subject to} && \frac{1}{2} \int_{\partial V} \big((\hat{\boldsymbol{k}} \times \hat{\boldsymbol{e}}^*) \times \boldsymbol{r} \big) \cdot \boldsymbol{J}(\boldsymbol{r}) \, \mathrm{dS} = 1 \\ & && \nabla \cdot \boldsymbol{J} = 0. \end{aligned} \tag{4.6}$$

Use the basis functions (3.1) to get the convex optimization problem

$$\begin{aligned} &\text{minimize} && \mathbf{J}^{\mathrm{H}}\mathbf{W}_{\mathrm{m}}^{(0)}\mathbf{J} \\ &\text{subject to} && \mathbf{f}_{\mathrm{m}}^{\mathrm{H}}\mathbf{J} = 1 \\ & && \mathbf{D}\mathbf{J} = \mathbf{0}, \end{aligned} \tag{4.7}$$

where $\mathbf{W}_{\mathrm{m}}^{(0)}$ is a $N \times N$ matrix for the stored magnetic energy, $\mathbf{D}$ a $N_1 \times N$ matrix representation of the divergence operator on the basis (3.1) and $\mathbf{f}_{\mathrm{m}}$ the corresponding

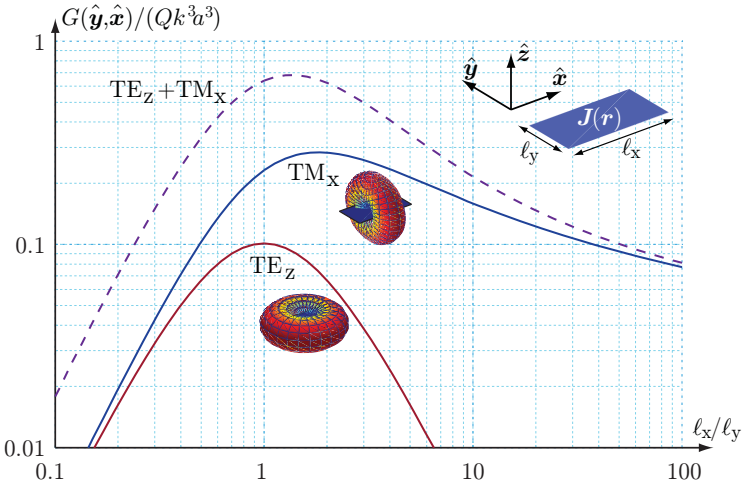

Figure 2: Upper bounds on the partial gain Q-factor quotient $G(\hat{\boldsymbol{y}},\hat{\boldsymbol{x}})/Q$ for currents confined to planar rectangles with sides ℓ_x and ℓ_y for small antennas using (4.4) and (4.8). The bound is normalized with k^3a^3, where a is the radius of the smallest circumscribing sphere, *i.e.*, $a = (\ell_x^2 + \ell_y^2)^{1/2}/2$.

row matrix for the first constraint in (4.6). Use Lagrange multipliers, ν_1 and $\boldsymbol{\nu}_2$, to transform (4.7) to the linear system

$$\begin{pmatrix} \mathbf{W}_{\mathrm{m}}^{(0)} & \mathbf{f}_{\mathrm{m}} & \mathbf{D}^{\mathrm{H}} \\ \mathbf{f}_{\mathrm{m}}^{\mathrm{H}} & 0 & \mathbf{0} \\ \mathbf{D} & \mathbf{0} & \mathbf{0} \end{pmatrix} \begin{pmatrix} \boldsymbol{\rho} \\ \nu_1 \\ \boldsymbol{\nu}_2 \end{pmatrix} = \begin{pmatrix} \mathbf{0} \\ 1 \\ \mathbf{0} \end{pmatrix}. \tag{4.8}$$

In [14], it is also shown that the constraint on G/Q is relaxed for combined electric and magnetic dipole antennas:

$$\frac{G}{Q} \leq \left(\sqrt{\frac{G_{\mathrm{e}}}{Q_{\mathrm{e}}}} + \sqrt{\frac{G_{\mathrm{m}}}{Q_{\mathrm{m}}}} \right)^2. \tag{4.9}$$

We consider a planar rectangle to illustrate the physical bounds on G/Q for small antennas, see Fig. 2. The rectangle has side lengths ℓ_x and ℓ_y with the radius $a = (\ell_x^2+\ell_y^2)^{1/2}/2$ of the smallest circumscribing sphere. The bound on the electric dipole is identical to the results in [12–14] and many small dipole antennas perform close to the bound [13]. The magnetic dipole case is more restricted. In particular, the bound shows that it is difficult to utilize the magnetic dipole for elongated structures. The combined mode case (4.9) offers a substantially improved performance [14].

The bounds in Fig. 2 are computed using piecewise linear basis functions on rectangular elements. We use a non-equidistant mesh for the electric dipole case, where the mesh is constructed to have approximately equal charge on each element for improved convergence. The magnetic dipole case is computed on an equidistant mesh. We also use the constraint $\mathbf{DJ} = \mathbf{0}$ to reduce the size of the linear system.

4.2 Maximal G/Q

Maximization of G/Q for finite sized antennas is formulated as a convex optimization problem. Combine (2.4) and (2.5) to express the gain Q-factor quotient as

$$\frac{G(\hat{\boldsymbol{k}},\hat{\boldsymbol{e}})}{Q} = \frac{2\pi P(\hat{\boldsymbol{k}},\hat{\boldsymbol{e}})}{\mathrm{c}_0 k \max\{\widetilde{W}_{\mathrm{vac}}^{(\mathrm{e})},\widetilde{W}_{\mathrm{vac}}^{(\mathrm{m})}\}}. \tag{4.10}$$

In [14], the D/Q quotient is maximized for the case with $w^{(\mathrm{e})} \geq w^{(\mathrm{m})}$ using a Lagrangian formulation. To instead obtain a convex optimization problem we rewrite the quotient G/Q as a constrained optimization problem. We follow [14] and note that G/Q is invariant for multiplicative scalings $\boldsymbol{J} \to \alpha\boldsymbol{J}$ with arbitrary complex valued $\alpha \neq 0$. It is hence sufficient to consider real-valued quantities $\hat{\boldsymbol{e}}^* \cdot \boldsymbol{F} \approx \mathbf{F}^{\mathrm{H}}\mathbf{J}$, see (3.2). Moreover, maximization of $P \sim |\mathbf{F}^{\mathrm{H}}\mathbf{J}|^2$ can be replaced by maximization of $\mathrm{Re}\{\mathbf{F}^{\mathrm{H}}\mathbf{J}\}$. This gives the convex optimization problem

$$\begin{aligned} &\text{maximize} && \mathrm{Re}\{\mathbf{F}^{\mathrm{H}}\mathbf{J}\} \\ &\text{subject to} && \mathbf{J}^{\mathrm{H}}\mathbf{W}_{\mathrm{e}}\mathbf{J} \leq 1 \\ &&& \mathbf{J}^{\mathrm{H}}\mathbf{W}_{\mathrm{m}}\mathbf{J} \leq 1. \end{aligned} \tag{4.11}$$

This is a quadratically constrained linear program (QCLP) giving the upper bound on (4.10) as $G/Q \leq p_1^2 k^3$, where $p_1 = \mathrm{Re}\{\mathbf{F}^{\mathrm{H}}\mathbf{J}\}$ and $\mathbf{J}$ a solution of (4.11). Note, that the current matrix, $\mathbf{J}$, is rescaled such that $\mathbf{J}^{\mathrm{H}}\mathbf{W}_{\mathrm{m}}\mathbf{J}$ is dimensionless.

There are many alternative convex formulations to maximize (4.10), *e.g.*, the Lagrange dual or using that the maximum of two convex functions is convex [5] to minimize the stored energy, *i.e.*,

$$\begin{aligned} &\text{minimize} && \max\{\mathbf{J}^{\mathrm{H}}\mathbf{W}_{\mathrm{e}}\mathbf{J}, \mathbf{J}^{\mathrm{H}}\mathbf{W}_{\mathrm{m}}\mathbf{J}\} \\ &\text{subject to} && \mathrm{Re}\{\mathbf{F}^{\mathrm{H}}\mathbf{J}\} = 1 \end{aligned} \tag{4.12}$$

giving $G/Q \leq k^3 p_2^{-1}$, where $p_2 = \max\{\mathbf{J}^{\mathrm{H}}\mathbf{W}_{\mathrm{e}}\mathbf{J}, \mathbf{J}^{\mathrm{H}}\mathbf{W}_{\mathrm{m}}\mathbf{J}\}$ and $\mathbf{J}$ a solution of (4.12).

We consider currents confined to planar rectangles to illustrate the results. The bound on G/Q and its corresponding Q and D for lossless antennas are depicted in Fig. 3 for rectangles with side lengths ℓ_{x} and $\ell_{\mathrm{y}} = \{0.5, 0.2, 0.1, 0.001\}\ell_{\mathrm{x}}$. The partial gain is evaluated for the polarization $\hat{\boldsymbol{e}} = \hat{\boldsymbol{x}}$ and the directions $\hat{\boldsymbol{k}} = \hat{\boldsymbol{z}}$ and $\hat{\boldsymbol{k}} = \hat{\boldsymbol{y}}$. The two optimization formulations (4.11) and (4.12) give similar results when solved using `CVX` [10]. The bound on G/Q is normalized with the electrical size k^3a^3 to simplify comparison with the results in [13, 14], where a denotes the radius of the smallest circumscribing sphere. The low-frequency limit for $\hat{\boldsymbol{k}} = \hat{\boldsymbol{z}}$ is given by the polarizability as shown in [14]. It is also observed that $G/(Qk^3a^3)$ is almost independent of the electrical size $\ell_{\mathrm{x}}/\lambda$ for $\ell_{\mathrm{x}}/\lambda < 0.33$ or $ka < 1$.

The case with radiation in the $\hat{\boldsymbol{k}} = \hat{\boldsymbol{y}}$ direction offers an increased G/Q. In particular, the $\ell_{\mathrm{y}} = 0.5\ell_{\mathrm{x}}$ case increases G/Q from 0.29 to 0.63. Here, we note that the bound in [11–13] is sharper for this case. It is also important to realize that the bound in [11–13] are for the bandwidth of the antenna and it is not guaranteed that the optimal current distributions considered here can be generated from single-port

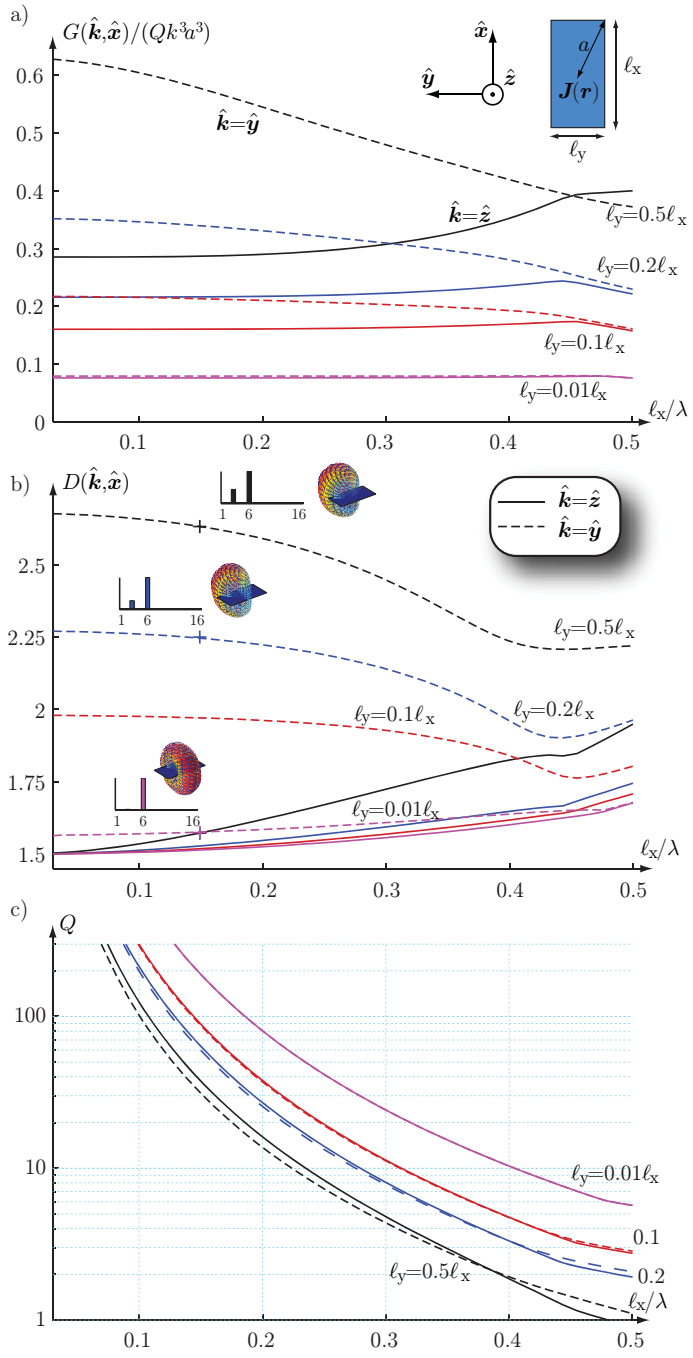

Figure 3: Upper bounds on the partial gain Q-factor quotient $G(\hat{\boldsymbol{k}},\hat{\boldsymbol{x}})/Q$ for currents confined to planar rectangles with sides ℓ_x and $\ell_y = \{0.5, 0.2, 0.1, 0.01\}\ell_x$ for $\hat{\boldsymbol{k}} = \{\hat{\boldsymbol{y}}, \hat{\boldsymbol{z}}\}$ using (4.11). The bound is normalized with k^3a^3, where a is the radius of the smallest circumscribing sphere, *i.e.*, $a = (\ell_x^2 + \ell_y^2)^{1/2}/2$. a) maximal G/Q. bc) resulting D and Q for lossless antennas.

antennas with a half-power fractional bandwidth $B \approx 2/Q$, see also [16]. In Fig. 3a, it is further seen that the improvement for the $\hat{\boldsymbol{k}} = \hat{\boldsymbol{y}}$ direction diminishes as $\ell_{\rm y}$ decreases.

The corresponding partial directivities, $D(\hat{\boldsymbol{k}}, \hat{\boldsymbol{x}})$, and Q-factors for lossless structures are depicted in Figs 3bc, respectively. Here, it is observed that the directivity differs between the $\hat{\boldsymbol{k}} = \hat{\boldsymbol{z}}$ and $\hat{\boldsymbol{k}} = \hat{\boldsymbol{y}}$ cases. There is also a decrease in the Q for the $\hat{\boldsymbol{k}} = \hat{\boldsymbol{y}}$ case except for the larger structures, $\ell_{\rm x}/\lambda > 0.4$, where Q is very low.

We expand the far-field in spherical modes to analyze the radiated field, see App. B. It is noted that the radiation pattern for the $\hat{\boldsymbol{k}} = \hat{\boldsymbol{z}}$ case is dominated by mode number $\nu = 6$, *i.e.*, $\mathrm{TM_x}$ or an $\hat{\boldsymbol{x}}$-directed electric dipole (B.3). There are also small contributions from higher order modes as analyzed in Sec. 4.4. The improved performance for the $\hat{\boldsymbol{k}} = \hat{\boldsymbol{y}}$ case is due to the additional excitation of a $\hat{\boldsymbol{z}}$-directed magnetic dipole, $\nu = 3$ ($\mathrm{TE_z}$). This is consistent with the explicit solution for small mixed mode antennas in (4.9), see also [14].

4.3 Maximal G/Q for $D \geq D_0$

The Chu bound [8] shows that the radiation is dominated by dipole modes for small antennas $ka \ll 1$. Consequently, the directivity is low, *i.e.*, $D \approx 3/2$ for single mode antennas and in general bounded as $D \leq 3$ for mixed electric and magnetic dipole modes. Higher directivity requires higher order modes that imply a higher Q, *e.g.*, the Q of quadrupole modes is proportional to $(ka)^{-5}$ for $ka \ll 1$. It is hence interesting to investigate the G/Q bound for antennas with directivities $D \geq D_0$ for some $D_0 > 3/2$. These bounds give an estimate of the increased Q-factor for superdirective antennas [2, 3, 19].

The partial directivity (2.3) is included in the optimization problem (4.12) with the constraint $P_{\rm rad} \leq 4\pi P(\hat{\boldsymbol{k}}, \hat{\boldsymbol{e}}) D_0^{-1}$ giving

$$\begin{aligned} \text{minimize} \quad & \max\{\mathbf{J}^{\rm H}\mathbf{W}_{\rm e}\mathbf{J}, \mathbf{J}^{\rm H}\mathbf{W}_{\rm m}\mathbf{J}\} \\ \text{subject to} \quad & \mathrm{Re}\{\mathbf{F}^{\rm H}\mathbf{J}\} = 1 \\ & \mathbf{J}^{\rm H}\mathbf{P}\mathbf{J} \leq k^3 D_0^{-1}, \end{aligned} \tag{4.13}$$

where the factor $k^3 D_0^{-1}$ is due to the normalization of $\mathbf{P}$ and $\mathbf{F}$.

The bounds are illustrated in Fig 4 for planar rectangles with $\ell_{\rm y} = 0.5\ell_{\rm x}$ and for the polarization $\hat{\boldsymbol{e}} = \hat{\boldsymbol{x}}$. The constraints $D_0 = \{1.7, 1.8\}$ and $D_0 = \{3, 3.2\}$ are considered for $\hat{\boldsymbol{k}} = \hat{\boldsymbol{z}}$ and $\hat{\boldsymbol{k}} = \hat{\boldsymbol{y}}$, respectively. The addition of the constraints reduce G/Q for small structures when the constraint is active. The resulting partial directivities are seen in Fig 4b together with the modal distribution for $\ell_{\rm x}/\lambda \approx 0.15$. The superdirectivity for the $D_0 = \{1.7, 1.8\}$ cases are due to the excitation of electric quadrupole terms. This also explains the increased Q-factors.

Fig. 5 illustrates the corresponding results for Q using $D_0 = 10$ and radiation in the $\hat{\boldsymbol{k}} = \{\hat{\boldsymbol{x}}, \hat{\boldsymbol{y}}, \hat{\boldsymbol{z}}\}$ directions with polarizations $\hat{\boldsymbol{e}} = \{\hat{\boldsymbol{y}}, \hat{\boldsymbol{x}}, \hat{\boldsymbol{x}}\}$ for a lossless structure. Here, the cost of superdirectivity is clearly seen. The Q-factor is highest for the $\hat{\boldsymbol{k}} = \hat{\boldsymbol{z}}$ case where the symmetry causes the current to radiate in both the $\hat{\boldsymbol{z}}$ and $-\hat{\boldsymbol{z}}$ directions. The mode expansion indicates that many higher order modes are

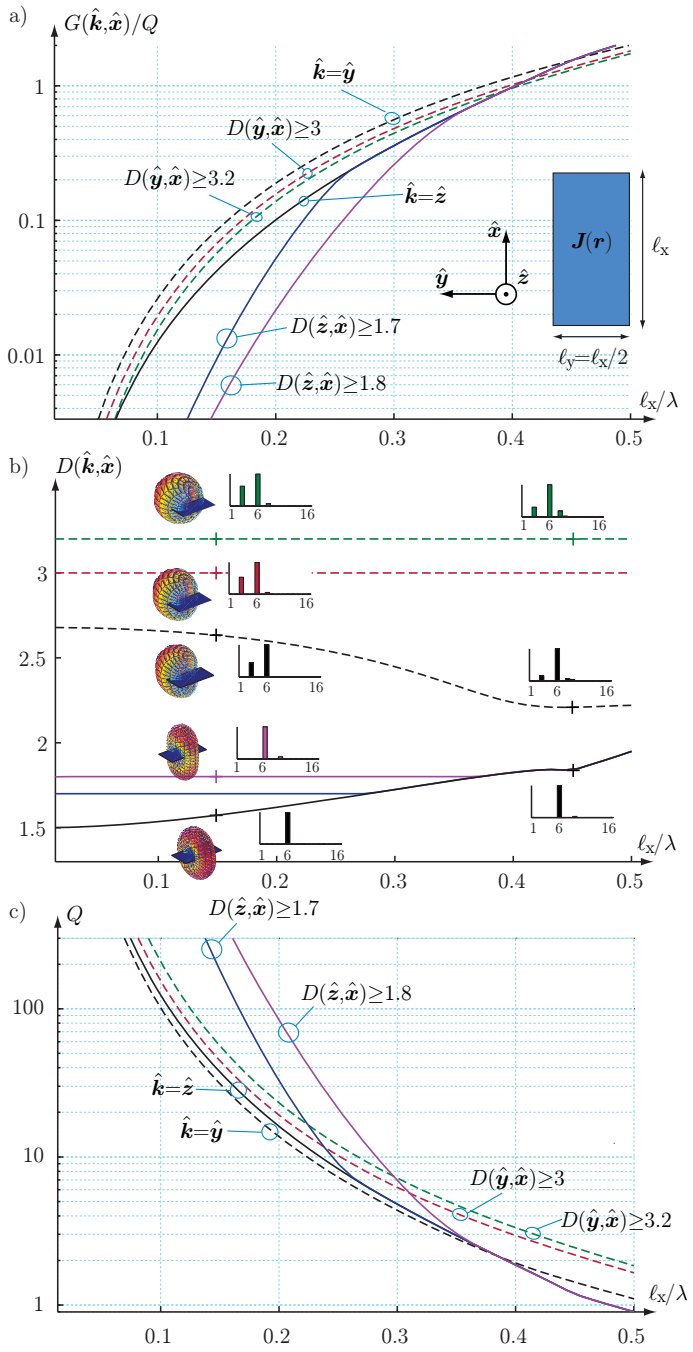

Figure 4: Upper bounds on the partial gain Q-factor quotient for antennas with $D(\hat{\boldsymbol{k}},\hat{\boldsymbol{e}}) \geq D_0$ for a planar rectangle with side lengths ℓ_x and $\ell_y = \ell_x/2$. a) G/Q. bc) resulting D and Q for lossless antennas.

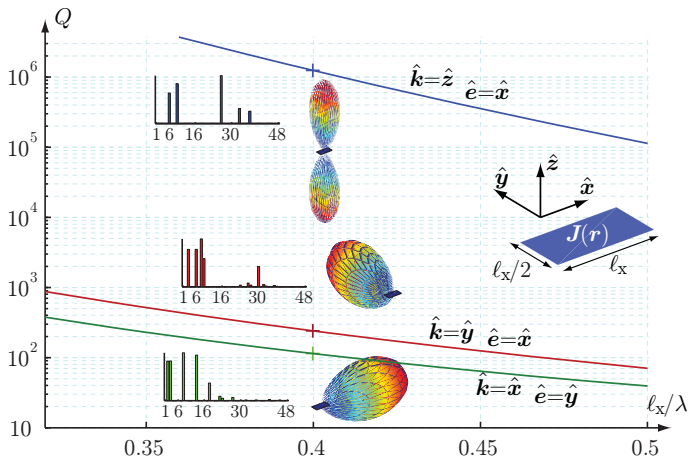

Figure 5: Lower bound on the Q-factor for lossless superdirective antennas having $D(\hat{\boldsymbol{k}}, \hat{\boldsymbol{e}}) \geq D_0 = 10$ constrained to a planar rectangle with side lengths ℓ_x and $\ell_y = \ell_x/2$ using (4.13).

excited. The $\hat{\boldsymbol{k}} = \{\hat{\boldsymbol{x}}, \hat{\boldsymbol{y}}\}$ cases have pencil beams and much lower Q factors. The end-fire case $\hat{\boldsymbol{k}} = \hat{\boldsymbol{x}}$ has the lowest Q with $Q \approx 100$ for $\ell_x \approx 0.4\lambda$.

4.4 Minimal Q for given radiation pattern

Consider the case with a desired radiation pattern, $\boldsymbol{F}_0(\hat{\boldsymbol{k}})$. We search for a current density such that $\boldsymbol{F} \approx \boldsymbol{F}_0$, with minimal stored energy. The deviation of $\boldsymbol{F}$ from $\boldsymbol{F}_0$ can be quantified by the projection of $\boldsymbol{F}$ on $\boldsymbol{F}_0$ or by some norm $||\boldsymbol{F} - \boldsymbol{F}_0||$. We start by maximizing $\boldsymbol{F}$ projected on $\boldsymbol{F}_0$, *i.e.*, the real valued part of

$$\int_\Omega \boldsymbol{F}_0(\hat{\boldsymbol{k}}) \cdot \boldsymbol{F}^*(\hat{\boldsymbol{k}}) \, \mathrm{d}\Omega_{\hat{\boldsymbol{k}}} = \int_V \boldsymbol{J}^*(\boldsymbol{r}) \cdot \boldsymbol{J}_0(\boldsymbol{r}) \, \mathrm{dV} \approx \mathbf{J}^{\mathrm{H}} \mathbf{J}_0, \tag{4.14}$$

where Ω denotes the unit sphere and

$$\boldsymbol{J}_0(\boldsymbol{r}) = \int_\Omega \boldsymbol{F}_0(\hat{\boldsymbol{k}}) \mathrm{e}^{\mathrm{j}k\hat{\boldsymbol{k}}\cdot\boldsymbol{r}} \, \mathrm{d}\Omega_{\hat{\boldsymbol{k}}} \tag{4.15}$$

is the desired current density on the structure.

This gives the convex optimization problem

$$\begin{aligned} \text{maximize} \quad & \mathrm{Re}\{\mathbf{J}_0^{\mathrm{H}} \mathbf{J}\} \\ \text{subject to} \quad & \mathbf{J}^{\mathrm{H}} \mathbf{W}_{\mathrm{e}} \mathbf{J} \leq 1 \\ & \mathbf{J}^{\mathrm{H}} \mathbf{W}_{\mathrm{m}} \mathbf{J} \leq 1. \end{aligned} \tag{4.16}$$

It is common to expand the radiated far field in spherical vector harmonics, $\boldsymbol{A}_\nu$, or modes, see App. B, *i.e.*,

$$\boldsymbol{F}_0(\hat{\boldsymbol{k}}) = 4\pi \sum_{\nu=1}^{N_\nu} f_{0,\nu} \mathrm{j}^{l+1-\tau} \boldsymbol{A}_\nu(\hat{\boldsymbol{k}}), \tag{4.17}$$

where N_ν is sufficiently large [18] and the expansion coefficients are

$$f_{0,\nu} = \frac{\mathrm{j}^{\tau-l-1}}{4\pi} \int_\Omega \boldsymbol{A}_\nu(\hat{\boldsymbol{k}}) \cdot \boldsymbol{F}_0(\hat{\boldsymbol{k}}) \,\mathrm{d}\Omega_{\hat{\boldsymbol{k}}} \tag{4.18}$$

and similarly for the expansion coefficients f_ν of $\boldsymbol{F}$. Here, the multiindex $\nu = \{\tau, s, m, l\}$ for $l = 1, 2, \ldots$, $s = 1, 2$, $m = 0, 1, \ldots, l$, and $\tau = 1, 2$ is introduced to simplify the notation. The index, ν, is also ordered such that $\nu = 2(l^2 + l - 1 + (-1)^s m) + \tau$, see App. B. The current in (4.16) is

$$\boldsymbol{J}_0(\boldsymbol{r}) = \sum_{\nu=1}^{N_\nu} f_{0,\nu} \int_\Omega \boldsymbol{A}_\nu(\hat{\boldsymbol{k}}) \mathrm{e}^{\mathrm{j}k\hat{\boldsymbol{k}}\cdot\boldsymbol{r}} \,\mathrm{d}\Omega_{\hat{\boldsymbol{k}}} = \sum_{\nu=1}^{N_\nu} f_{0,\nu} \boldsymbol{v}_\nu(k\boldsymbol{r}), \tag{4.19}$$

where $\boldsymbol{v}_\nu(k\boldsymbol{r})$ denotes the regular spherical vector waves, see App. B.

We can also minimize the stored energy for a radiated field of the form $\boldsymbol{F}_0(\hat{\boldsymbol{k}})$, *i.e.*,

$$\begin{aligned} &\text{minimize} \quad \max\{\mathbf{J}^{\mathrm{H}}\mathbf{W}_{\mathrm{e}}\mathbf{J}, \mathbf{J}^{\mathrm{H}}\mathbf{W}_{\mathrm{m}}\mathbf{J}\} \\ &\text{subject to} \quad \left(\int_\Omega |\boldsymbol{F}(\hat{\boldsymbol{k}}) - \boldsymbol{F}_0(\hat{\boldsymbol{k}})|^2 \,\mathrm{d}\Omega_{\hat{\boldsymbol{k}}}\right)^{1/2} < 4\pi\delta, \end{aligned} \tag{4.20}$$

where δ quantifies the deviation of the desired radiation pattern and the least-square norm is used for simplicity. It is convenient to expand the radiated field in spherical vector waves and rewrite the deviation as

$$\int_\Omega |\boldsymbol{F}(\hat{\boldsymbol{k}}) - \boldsymbol{F}_0(\hat{\boldsymbol{k}})|^2 \,\mathrm{d}\Omega_{\hat{\boldsymbol{k}}} = (4\pi)^2 \sum_{\nu=1}^{N_\nu} |f_\nu - f_{0,\nu}|^2, \tag{4.21}$$

where

$$\begin{aligned} f_\nu = \int_\Omega \boldsymbol{A}_\nu(\hat{\boldsymbol{k}}) \cdot \boldsymbol{F}(\hat{\boldsymbol{k}}) \,\mathrm{d}\Omega_{\hat{\boldsymbol{k}}} &= \int_V \boldsymbol{J}(\boldsymbol{r}) \cdot \int_\Omega \boldsymbol{A}_\nu(\hat{\boldsymbol{k}}) \mathrm{e}^{\mathrm{j}k\hat{\boldsymbol{k}}\cdot\boldsymbol{r}} \,\mathrm{d}\Omega_{\hat{\boldsymbol{k}}} \,\mathrm{dV} \\ &= \int_V \boldsymbol{J}(\boldsymbol{r}) \cdot \boldsymbol{v}_\nu(k\boldsymbol{r}) \,\mathrm{dV}. \end{aligned} \tag{4.22}$$

This gives the optimization problem

$$\begin{aligned} &\text{minimize} \quad \max\{\mathbf{J}^{\mathrm{H}}\mathbf{W}_{\mathrm{e}}\mathbf{J}, \mathbf{J}^{\mathrm{H}}\mathbf{W}_{\mathrm{m}}\mathbf{J}\} \\ &\text{subject to} \quad \left(\sum_{\nu=1}^{N_\nu} |f_\nu - f_{0,\nu}|^2\right)^{1/2} < \delta \\ &\qquad\qquad f_n = \int_V \boldsymbol{J}(\boldsymbol{r}) \cdot \boldsymbol{v}_n(k\boldsymbol{r}) \,\mathrm{dV}. \end{aligned} \tag{4.23}$$

It is noted that arbitrary weight functions and norms can be used in (4.23).

A planar rectangle with $\ell_{\mathrm{y}} = \ell_{\mathrm{x}}/2$ is considered to illustrate the results for given far-fields (4.16) and (4.23). The Q factors are depicted in Fig. 6 for projections (4.16)

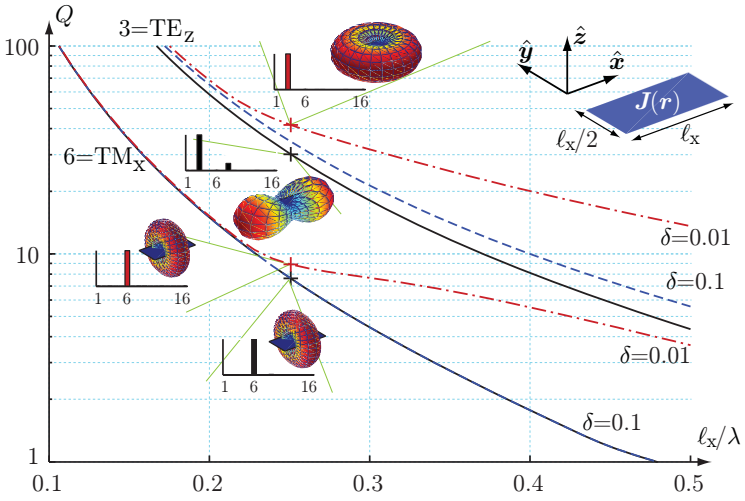

Figure 6: Q-factors for a lossless planar rectangle (side lengths ℓ_x and $\ell_x/2$) with electric (TM_x) and magnetic (TE_z) dipole radiation patterns using (4.16) and (4.23).

and norm bounds (4.23) for the cases of the $\hat{\boldsymbol{x}}$-directed electric dipole (TM_x) and $\hat{\boldsymbol{z}}$-directed magnetic dipole (TE_z) patterns.

We observe that the Q is lower for the electric dipole mode than the magnetic dipole mode. The Q is also lowest for the projection cases (4.16). Moreover, Q tend to increase as δ decreases, *i.e.*, the lowest Q is for radiation patterns that are close to but not exact dipoles. The radiation patterns are depicted for $\ell_x/\lambda \approx 0.25$. It is hard to distinguish between the patterns for the TM_x cases, but the partial directivity for the projection case and $\delta = 0.1$ is lower than for $D(\hat{\boldsymbol{z}}, \hat{\boldsymbol{x}})$ for the $\delta = 0.01$ case in the region around $\ell_x/\lambda \approx 0.25$. The radiation patterns differ more for the TE_z case, where again the projection formulation (4.16) offers the lowest Q.

4.5 Embedded antennas

It is useful to analyze the case when the antenna is embedded in a structure. In this case the currents on the entire structure, V, contribute to the radiation but we can only control the currents in the volume $V_1 \subset V$, see Fig. 1. Here, we consider the case where the structure $V_2 = V - V_1$ is perfectly electric conducting (PEC), see Fig. 7. The induced currents on the surface of V_2 are determined from the electric field integral equation (EFIE) that has the matrix elements [23]

$$Z_{mn} = \int_{\partial V}\int_{\partial V} \Big(k^2 \boldsymbol{\psi}_m(\boldsymbol{r}_1)\cdot\boldsymbol{\psi}_n(\boldsymbol{r}_2) - \nabla_1\cdot\boldsymbol{\psi}_m(\boldsymbol{r}_1)\nabla_2\cdot\boldsymbol{\psi}_n(\boldsymbol{r}_2)\Big)\frac{\mathrm{e}^{-\mathrm{j}k|\boldsymbol{r}_1-\boldsymbol{r}_2|}}{|\boldsymbol{r}_1-\boldsymbol{r}_2|}\,\mathrm{dS}_1\,\mathrm{dS}_2, \quad (4.24)$$

where the similarities with (2.6), (2.7), (2.8), and (3.4) are noted. The integration in (4.24) is over the PEC surface of the structure. The driving sources of the EFIE

are confined to the region V_1 and they are unknown. Moreover the EFIE is not necessarily valid in V_1. Decompose the current density as $\mathbf{J}^{\mathrm{T}} = [\mathbf{J}_1^{\mathrm{T}}\ \mathbf{J}_2^{\mathrm{T}}]$, where $\mathbf{J}_n$ is the current density in V_n, $n = 1, 2$. Assuming driving voltages $\mathbf{V}$ in the region V_1 gives the linear system

$$\begin{pmatrix} \mathbf{Z}_{11} & \mathbf{Z}_{12} \\ \mathbf{Z}_{21} & \mathbf{Z}_{22} \end{pmatrix} \begin{pmatrix} \mathbf{J}_1 \\ \mathbf{J}_2 \end{pmatrix} = \begin{pmatrix} \mathbf{V} \\ \mathbf{0} \end{pmatrix}. \tag{4.25}$$

Here, the first row is unknown but the second row gives the constraint

$$\mathbf{Z}_{21}\mathbf{J}_1 + \mathbf{Z}_{22}\mathbf{J}_2 = \mathbf{0} \tag{4.26}$$

that can be added as a constraint to the convex optimization problems in this paper, *e.g.*, the G/Q bound in (4.11).

It is convenient to use (4.26) to express the induced current densities $\mathbf{J}_2$ in $\mathbf{J}_1$, *i.e.*,

$$\mathbf{J}_2 = -\mathbf{Z}_{22}^{-1}\mathbf{Z}_{21}\mathbf{J}_1 = \mathbf{Z}'\mathbf{J}_1 \tag{4.27}$$

and eliminate $\mathbf{J}_2$ in the optimization problem. Decompose the matrices $\mathbf{W}_{\mathrm{e}}$ and $\mathbf{W}_{\mathrm{m}}$ according to

$$\mathbf{W} = \begin{pmatrix} \mathbf{W}_{11} & \mathbf{W}_{12} \\ \mathbf{W}_{21} & \mathbf{W}_{22} \end{pmatrix} \tag{4.28}$$

that gives

$$\begin{aligned} \mathbf{J}^{\mathrm{H}}\mathbf{W}\mathbf{J} &= \mathbf{J}_1^{\mathrm{H}}\mathbf{W}_{11}\mathbf{J}_1 + \mathbf{J}_1^{\mathrm{H}}\mathbf{W}_{12}\mathbf{J}_2 + \mathbf{J}_2^{\mathrm{H}}\mathbf{W}_{21}\mathbf{J}_1 + \mathbf{J}_2^{\mathrm{H}}\mathbf{W}_{22}\mathbf{J}_2 \\ &= \mathbf{J}_1^{\mathrm{H}}\big(\mathbf{W}_{11} + 2\,\mathrm{Re}\{\mathbf{W}_{12}\mathbf{Z}'\} + \mathbf{Z}'^{\mathrm{H}}\mathbf{W}_{22}\mathbf{Z}'\big)\mathbf{J}_1 = \mathbf{J}_1^{\mathrm{H}}\mathbf{W}'\mathbf{J}_1 \end{aligned} \tag{4.29}$$

and

$$\mathbf{F}^{\mathrm{H}}\mathbf{J} = \mathbf{F}_1^{\mathrm{H}}\mathbf{J}_1 + \mathbf{F}_2^{\mathrm{H}}\mathbf{J}_2 = \mathbf{F}_1^{\mathrm{H}}\mathbf{J}_1 + \mathbf{F}_2^{\mathrm{H}}\mathbf{Z}'\mathbf{J}_1 = \mathbf{F}'^{\mathrm{H}}\mathbf{J}. \tag{4.30}$$

The optimization problem on G/Q becomes

$$\begin{aligned} \text{maximize} \quad & \mathrm{Re}\{\mathbf{F}'^{\mathrm{H}}\mathbf{J}_1\} \\ \text{subject to} \quad & \mathbf{J}_1^{\mathrm{H}}\mathbf{W}'_{\mathrm{e}}\mathbf{J}_1 \le 1 \\ & \mathbf{J}_1^{\mathrm{H}}\mathbf{W}'_{\mathrm{m}}\mathbf{J}_1 \le 1. \end{aligned} \tag{4.31}$$

We illustrate the bound on G/Q, normalized with k^3a^3, for embedded antennas using the structures in Fig. 7. The strip dipole in Fig. 7a has length ℓ_{x} and width $\ell_{\mathrm{y}} = \ell_{\mathrm{x}}/100$. Let the center, $|x| \le \xi\ell_{\mathrm{x}}$ be the region, V_1, where the currents are optimized. We observe that the performance decreases with decreasing ξ except for $\ell_{\mathrm{x}}/\lambda \approx 0.5$, where the center fed strip dipole is self-resonant. This shows that the induced currents are optimal for short dipoles. This is consistent with the analysis of strip dipoles in [14].

The second example is for antennas embedded in a PEC planar rectangle with length ℓ_{x} and width $\ell_{\mathrm{y}} = \ell_{\mathrm{x}}/2$. We consider the cases with feed currents in either rectangular regions in the upper corner or in a strip on the side of the structure, see 7b. The G/Q quotient is optimized for $\hat{\boldsymbol{k}} = \hat{\boldsymbol{z}}$ and $\hat{\boldsymbol{e}} = \hat{\boldsymbol{x}}$ using (4.31). We observe that the performance deteriorates for small regions and small antennas. There is however a region around $\ell_{\mathrm{x}}/\lambda = 0.37$ where performance is close to the case of using the entire structure.

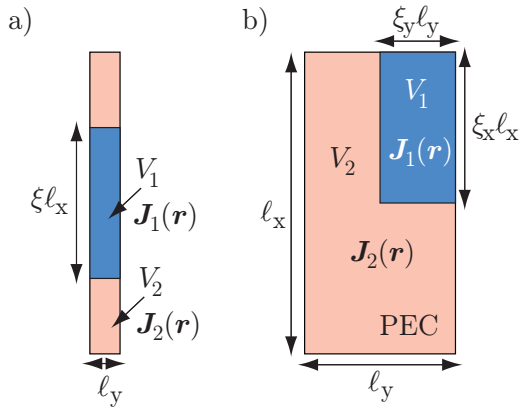

Figure 7: Illustration of embedded antennas in planar metallic rectangles. Arbitrary currents $\boldsymbol{J}_1(\boldsymbol{r})$ in V_1 and induced currents $\boldsymbol{J}_2(\boldsymbol{r})$ in V_2. a) antenna region in the center. b) antenna region in the upper corner.

5 Conclusions

We show that several performance bounds for antennas can be formulated as convex optimization problems. Standard software [5, 10] is used to solve the convex optimization problems. The results for D/Q are consistent with the bounds in [13, 14]. The new bounds offer physical insight to the design of small antennas, see also [14]. They also offer the possibility of systematic studies of how Q and directivity are related for small superdirective antennas. Moreover, properties of antennas embedded in structures, such as mobile phones and other terminals, are discussed.

It is important to realize that the convex optimization problem determines an optimal current distribution. This current is in general not unique although the minimum of the convex optimization problems is unique. It is also not known if there are antennas performing close to the bounds except for the case of electric dipole type antennas [13]. Moreover, the optimal performance can be useful in global optimization of antennas.

Appendix A Polarizability

The physical bounds on D/Q in [12, 13] are expressed in the polarizability of the antenna structure. In [14], it is also shown that the bound on small antennas (4.1) can be expressed in the polarizability. Here, we further show that the solution of the convex optimization problem (4.3) using (4.4) is identical to computing the polarizability [14] using Galerkin's method [24].

The polarizability for the polarization $\hat{\boldsymbol{e}}$ can be determined from the first moment of the induced normalized charge density ρ as

$$\int_{\partial V} \hat{\boldsymbol{e}}^* \cdot \boldsymbol{r}\rho(\boldsymbol{r}) \,\mathrm{dS} = E_0\gamma = E_0\hat{\boldsymbol{e}}^* \cdot \boldsymbol{\gamma}_\mathrm{e} \cdot \hat{\boldsymbol{e}}. \tag{A.1}$$

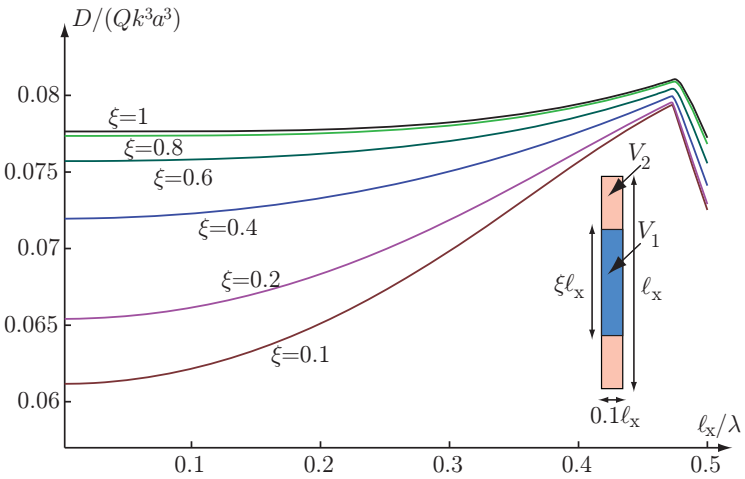

Figure 8: Bound on $G/(Qk^3a^3)$ for planar PEC strip dipoles with length ℓ_x and width $\ell_x/100$. Arbitrary currents in the central region, V_1 with length $\xi\ell_x$, of the strips for $\xi = 0.1, 0.2, 0.4, 0.6, 0.8, 1$.

Here, we keep the notation with complex conjugates on $\hat{\boldsymbol{e}}$ to simplify the comparison with (4.4), although it is sufficient to consider real valued unit vectors $\hat{\boldsymbol{e}}$ to determine the electrostatic polarizability. The charge density ρ is the solution of the integral equation

$$\int_{\partial V} \frac{\rho(\boldsymbol{r})}{4\pi|\boldsymbol{r}-\boldsymbol{r}'|}\,\mathrm{dS}' = E_0\hat{\boldsymbol{e}}\cdot\boldsymbol{r} + C, \quad \boldsymbol{r}\in\partial V, \tag{A.2}$$

where the constant C is determined from the constraint of zero total charge

$$\int_{\partial V} \rho(\boldsymbol{r})\,\mathrm{dS} = 0. \tag{A.3}$$

It turns out that it is convenient to set $E_0 = -\gamma^{-1}$ for comparison with (4.4). Expand the charge density in basis functions $\rho(\boldsymbol{r}) = \sum_{n=1}^{N}\rho_n\psi(\boldsymbol{r}) = \boldsymbol{\psi}^{\mathrm{T}}\boldsymbol{\rho}$, where $\boldsymbol{\psi}$ and $\boldsymbol{\rho}$ are $N\times 1$ matrices, to rewrite (A.1) as

$$\mathbf{f}^{\mathrm{H}}\boldsymbol{\rho} = E_0/\gamma = -1 \quad \text{where } \mathbf{f} = \int_{\partial V}(\hat{\boldsymbol{e}}\cdot\boldsymbol{r})\boldsymbol{\psi}(\boldsymbol{r})\,\mathrm{dS}. \tag{A.4}$$

Solving the integral equation (A.2) with the Galerkin's method [24] gives the linear system of equations

$$\mathbf{W}_{\mathrm{e}}^{(0)}\boldsymbol{\rho} = -\gamma^{-1}\mathbf{f} + C\mathbf{n}, \tag{A.5}$$

where the matrix $\mathbf{W}_{\mathrm{e}}^{(0)}$ is

$$\mathbf{W}_{\mathrm{e}}^{(0)} = \int_{\partial V}\int_{\partial V}\frac{\boldsymbol{\psi}(\boldsymbol{r})\boldsymbol{\psi}^{\mathrm{T}}(\boldsymbol{r}')}{4\pi|\boldsymbol{r}-\boldsymbol{r}'|}\,\mathrm{dS}\,\mathrm{dS}'. \tag{A.6}$$

Finally, the constraint (A.2) is

$$\mathbf{n}^{\mathrm{T}}\boldsymbol{\rho} = 0 \quad \text{where } \mathbf{n} = \int_{\partial V}\boldsymbol{\psi}(\boldsymbol{r})\,\mathrm{dS}. \tag{A.7}$$

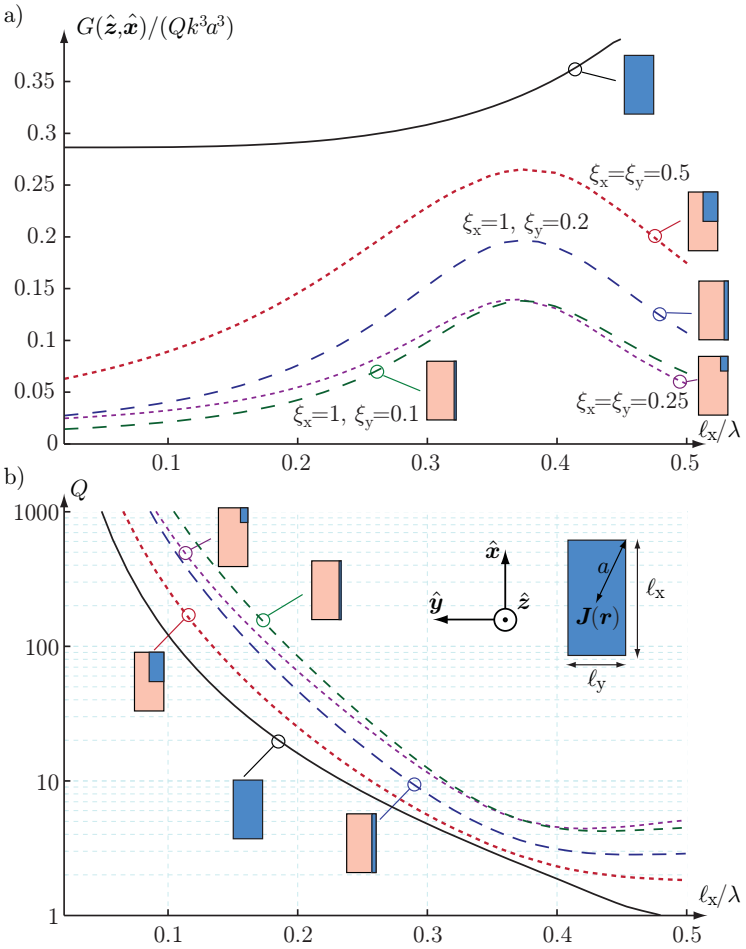

Figure 9: Bounds on G/Q and resulting Q for antennas embedded in planar metallic rectangles. Arbitrary currents $\boldsymbol{J}_1(\boldsymbol{r})$ in V_1 and induced currents $\boldsymbol{J}_2(\boldsymbol{r})$ in V_2 with the antenna region V_1 in the upper corner and on one edge, see Fig. 7b. a) bounds on G/Q using (4.31). b) resulting Q for a lossless structure.

Written as a linear system, (A.4), (A.5), and (A.7) becomes

$$\begin{pmatrix} \mathbf{W}_{\mathrm{e}}^{(0)} & \mathbf{f} & \mathbf{n} \\ \mathbf{f}^{\mathrm{H}} & 0 & 0 \\ \mathbf{n}^{\mathrm{H}} & 0 & 0 \end{pmatrix} \begin{pmatrix} \boldsymbol{\rho} \\ \gamma^{-1} \\ -C \end{pmatrix} = \begin{pmatrix} \mathbf{0} \\ -1 \\ 0 \end{pmatrix}. \tag{A.8}$$

We note that this system is identical to (4.4).

Appendix B Mode expansion

The radiated electromagnetic field $\boldsymbol{E}(\boldsymbol{r})$ is expanded in spherical vector waves [18] (or modes) outside a circumscribing sphere. The corresponding far field is expanded

in spherical vector harmonics as

$$\boldsymbol{E}(\boldsymbol{r}) \sim \mathrm{j}k\eta_0 \frac{\mathrm{e}^{-\mathrm{j}kr}}{4\pi r} \boldsymbol{F}(\hat{\boldsymbol{r}}) = \frac{\mathrm{e}^{-\mathrm{j}kr}}{kr} \sum_{\nu} b_\nu \mathrm{j}^{l+2-\tau} \boldsymbol{A}_\nu(\hat{\boldsymbol{r}}), \tag{B.1}$$

giving $f_\nu = b_\nu/(\eta_0 k^2)$ for the expansion coefficients in (4.22), where $\boldsymbol{r}$ is the spatial coordinate, $\hat{\boldsymbol{r}} = \boldsymbol{r}/r$, $r = |\boldsymbol{r}|$, and k the wavenumber. The multi index $\nu = \{\tau, s, m, l\}$ for $l = 1, 2, \ldots$, $s = 1, 2$, $m = 0, 1, \ldots, l$, and $\tau = 1, 2$ is introduced to simplify the notation. The index, ν, is also ordered such that $\nu = 2(l^2 + l - 1 + (-1)^s m) + \tau$, see [17].

There are a few alternative definitions of the spherical vector waves in the literature [4, 18, 20]. Here, we follow [20] and use $\cos m\phi$ and $\sin m\phi$ as basis functions in the azimuthal coordinate. This choice is motivated by the interpretation of the field related to the first 6 modes as the field from different Hertzian dipoles. For $\tau = 1, 2$, we use spherical vector harmonics

$$\mathbf{A}_{1sml}(\hat{\boldsymbol{r}}) = \frac{1}{\sqrt{l(l+1)}} \nabla \times \big(\boldsymbol{r}\, \mathrm{Y}_{sml}(\hat{\boldsymbol{r}})\big) \tag{B.2}$$

and $\mathbf{A}_{2sml}(\hat{\boldsymbol{r}}) = \hat{\boldsymbol{r}} \times \mathbf{A}_{1sml}(\hat{\boldsymbol{r}})$ where Y_{sml} denotes the spherical harmonics [4]. The modes labeled by $\tau = 1$ (odd ν) identify TE modes (or magnetic 2^l-poles) and the terms labeled by $\tau = 2$ (even ν) correspond to TM modes (or electric 2^l-poles). Moreover, the dipoles corresponding to $\nu = 1, 2$ are directed in the y-direction, $\nu = 3, 4$ in the z-direction, and $\nu = 5, 6$ in the x-direction having the explicit representation

$$\begin{cases} 1,\ \mathrm{TE_y}, & \boldsymbol{A}_{1111} = \beta(\hat{\boldsymbol{\theta}} \cos\phi - \hat{\boldsymbol{\phi}} \cos\theta \sin\phi) \\ 2,\ \mathrm{TM_y}, & \boldsymbol{A}_{2111} = \beta(\hat{\boldsymbol{\theta}} \cos\theta \sin\phi + \hat{\boldsymbol{\phi}} \cos\phi) \\ 3,\ \mathrm{TE_z}, & \boldsymbol{A}_{1201} = \beta(\hat{\boldsymbol{\phi}} \sin\theta) \\ 4,\ \mathrm{TM_z}, & \boldsymbol{A}_{2201} = \beta(-\hat{\boldsymbol{\theta}} \sin\theta) \\ 5,\ \mathrm{TE_x}, & \boldsymbol{A}_{1211} = \beta(-\hat{\boldsymbol{\theta}} \sin\phi - \hat{\boldsymbol{\phi}} \cos\theta \cos\phi) \\ 6,\ \mathrm{TM_x}, & \boldsymbol{A}_{2211} = \beta(\hat{\boldsymbol{\theta}} \cos\theta \cos\phi - \hat{\boldsymbol{\phi}} \sin\phi), \end{cases} \tag{B.3}$$

where $\beta = \sqrt{3/(8\pi)}$.

The regular, $\boldsymbol{v}_\nu$, spherical vector waves are given by

$$\boldsymbol{v}_{1sml}(k\boldsymbol{r}) = \mathrm{j}_l(kr)\, \mathbf{A}_{1sml}(\hat{\boldsymbol{r}}) \tag{B.4}$$

and $\boldsymbol{v}_{2sml} = k^{-1} \nabla \times \boldsymbol{v}_{1sml}$, where j_l denotes the spherical Bessel function.

References

[1] Antenna Standards Committee of the IEEE Antennas and Propagation Society. IEEE Standard Definitions of Terms for Antennas, 1993. IEEE Std 145-1993.

[2] D. Arceo and C. A. Balanis. A compact Yagi-Uda antenna with enhanced bandwidth. *IEEE Antennas and Wireless Propagation Letters*, **10**, 442–445, 2011.

[3] S. R. Best, E. E. Altshuler, A. D. Yaghjian, J. M. McGinthy, and T. H. O'Donnell. An impedance-matched 2-element superdirective array. *Antennas and Wireless Propagation Letters, IEEE*, **7**, 302–305, 2008.

[4] A. Boström, G. Kristensson, and S. Ström. Transformation properties of plane, spherical and cylindrical scalar and vector wave functions. In V. V. Varadan, A. Lakhtakia, and V. K. Varadan, editors, *Field Representations and Introduction to Scattering*, Acoustic, Electromagnetic and Elastic Wave Scattering, chapter 4, pages 165–210. Elsevier Science Publishers, Amsterdam, 1991.

[5] S. P. Boyd and L. Vandenberghe. *Convex optimization*. Cambridge Univ Pr, 2004.

[6] O. M. Bucci, G. D'Elia, G. Mazzarella, and G. Panariello. Antenna pattern synthesis: A new general approach. *Proceedings of the IEEE*, **82**(3), 358–371, 1994.

[7] J. Chalas, K. Sertel, and J. L. Volakis. Computation of the Q limits for arbitrary-shaped antennas using characteristic modes. In *Antennas and Propagation (APSURSI), 2011 IEEE International Symposium on*, pages 772–774. IEEE, 2011.

[8] L. J. Chu. Physical limitations of omni-directional antennas. *J. Appl. Phys.*, **19**, 1163–1175, 1948.

[9] W. Geyi. A method for the evaluation of small antenna Q. *IEEE Trans. Antennas Propagat.*, **51**(8), 2124–2129, 2003.

[10] M. Grant and S. Boyd. CVX: Matlab software for disciplined convex programming, version 1.21. `../../cvx`, April 2011.

[11] M. Gustafsson. Physical bounds on antennas of arbitrary shape. In *Antennas and Propagation Conference (LAPC), 2011 Loughborough*, pages 1–5. IEEE, 2011.

[12] M. Gustafsson, C. Sohl, and G. Kristensson. Physical limitations on antennas of arbitrary shape. *Proc. R. Soc. A*, **463**, 2589–2607, 2007.

[13] M. Gustafsson, C. Sohl, and G. Kristensson. Illustrations of new physical bounds on linearly polarized antennas. *IEEE Trans. Antennas Propagat.*, **57**(5), 1319–1327, May 2009.

[14] M. Gustafsson, M. Cismasu, and B. L. G. Jonsson. Physical bounds and optimal currents on antennas. *IEEE Trans. Antennas Propagat.*, 2012. in press.

[15] M. Gustafsson, M. Cismasu, and S. Nordebo. Physical bounds on small antennas as convex optimization problems. In *IEEE Antennas and Propagation Society International Symposium*, pages 1–2. IEEE, 2012.

[16] M. Gustafsson and S. Nordebo. Bandwidth, Q factor, and resonance models of antennas. *Progress in Electromagnetics Research*, **62**, 1–20, 2006.

[17] M. Gustafsson and S. Nordebo. Characterization of MIMO antennas using spherical vector waves. *IEEE Trans. Antennas Propagat.*, **54**(9), 2679–2682, 2006.

[18] J. E. Hansen, editor. *Spherical Near-Field Antenna Measurements*. Number 26 in IEE electromagnetic waves series. Peter Peregrinus Ltd., Stevenage, UK, 1988. ISBN: 0-86341-110-X.

[19] R. C. Hansen and R. E. Collin. *Small Antenna Handbook*. Wiley, 2011.

[20] R. F. Harrington. *Time Harmonic Electromagnetic Fields*. McGraw-Hill, New York, 1961.

[21] P. Hazdra, M. Capek, and J. Eichler. Radiation Q-factors of thin-wire dipole arrangements. *Antennas and Wireless Propagation Letters, IEEE*, **10**, 556–560, 2011.

[22] S. J. Orfanidis. Electromagnetic waves and antennas, 2002. `www.ece.rutgers.edu/~orfanidi/ewa`, revision date June 21, 2004.

[23] A. F. Peterson, S. L. Ray, and R. Mittra. *Computational Methods for Electromagnetics*. IEEE Press, New York, 1998.

[24] G. Strang. *Introduction to applied mathematics*. Wellesley-Cambridge Press, Box 157, Wellesley MA 02181, 1986.

[25] H. L. Thal. New radiation Q limits for spherical wire antennas. *IEEE Trans. Antennas Propagat.*, **54**(10), 2757–2763, October 2006.

[26] G. A. E. Vandenbosch. Reactive energies, impedance, and Q factor of radiating structures. *IEEE Trans. Antennas Propagat.*, **58**(4), 1112–1127, 2010.

[27] G. A. E. Vandenbosch. Simple procedure to derive lower bounds for radiation Q of electrically small devices of arbitrary topology. *IEEE Trans. Antennas Propagat.*, **59**(6), 2217–2225, 2011.

[28] J. Volakis, C. C. Chen, and K. Fujimoto. *Small Antennas: Miniaturization Techniques & Applications*. McGraw-Hill, New York, 2010.

[29] A. D. Yaghjian and H. R. Stuart. Lower bounds on the Q of electrically small dipole antennas. *IEEE Trans. Antennas Propagat.*, **58**(10), 3114–3121, 2010.